Published in final edited form as:
Anal Chem. 2009 November 1; 81(21): 9086–9095. doi:10.1021/ac9017692.

Quantitative measurement of zinc secretion from pancreatic islets with high temporal resolution using droplet-based microfluidics

Christopher J. Easley[1,†], **Jonathan V. Rocheleau**[1,‡], **W. Steven Head**[1], and **David W. Piston**[1,*]

[1] Vanderbilt University, Molecular Physiology and Biophysics, Vanderbilt University Medical Center, 702 Light Hall, Nashville, TN 37232, USA

Abstract

We assayed glucose-stimulated insulin secretion (GSIS) from live, murine islets of Langerhans in microfluidic devices by the downstream formation of aqueous droplets. Zinc ions, which are co-secreted with insulin from β-cells, were quantitatively measured from single islets with high temporal resolution using a fluorescent indicator, FluoZin-3. Real-time storage of secretions into droplets (volume of 0.470 ± 0.009 nL) effectively preserves the temporal chemical information, allowing reconstruction of the secretory time record. The use of passive flow control within the device removes the need for syringe pumps, requiring only a single handheld syringe. Under stimulatory glucose levels (11 mM), bursts of zinc as high as ~800 fg islet^{-1} min^{-1} were measured. Treatment with diazoxide effectively blocked zinc secretion, as expected. High temporal resolution reveals two major classes of oscillations in secreted zinc, with predominate periods at ~20-40 s and ~ 5-10 min. The more rapid oscillation periods match closely with those of intraislet calcium oscillations, while the slower oscillations are consistent with insulin pulses typically measured in bulk islet experiments or in the bloodstream. This droplet sampling technique should be widely applicable to time-resolved cellular secretion measurements, either in real-time or for post-processing.

Keywords

diabetes; cell imaging; islets of Langerhans; FluoZin-3; PDMS; confocal microscopy

Introduction

An electrically coupled cluster of multiple cell types[1-3], the pancreatic islet (~100-200 μm in diameter[4]) is a “micro-organ” that serves as the functional unit of insulin secretion, with the major task of maintaining blood glucose homeostasis. Defective or lost islet function is an underlying cause of diabetes and a common result of prolonged obesity or metabolic syndrome.[5] It has been shown that donor islets transplanted into the livers of patients with type I diabetes can result in complete insulin independence within weeks.[6] Recent studies have shown that subcutaneous islet transplants are capable of normalizing blood glucose homeostasis and achieving endocrine differentiation and vascularization.[7] Hence islets are capable of what appears to be normal function in an environment of non-native tissue.

* Address Correspondence to: David W. Piston, Ph.D. Department of Molecular Physiology and Biophysics Vanderbilt University Medical Center 735A Light Hall 21st Avenue South Nashville, TN 37232-0615, USA Phone: (615) 322-7030 Fax: (615) 322-7236 dave.piston@vanderbilt.edu.
†Current Address: 179 Chemistry Building Department of Chemistry and Biochemistry Auburn University Auburn, AL 36849, USA chris.easley@auburn.edu
‡Current Address: Institute of Biomaterials and Biomedical Engineering Departments of Medicine and Physiology University of Toronto Toronto, Ontario, Canada jrochele@uhnresearch.ca

As such, research on isolated islets is clearly warranted. Over the years, various insights have been gained through the use of optical[8] or fluorescence microscopy[9-10] of the tissue. However, few studies have focused on quantitative chemical analysis of secretion profiles of single islets, largely due to the difficulty of sampling and measuring secretions at such a small scale without incorporating many islets in the assay or greatly sacrificing temporal resolution.[11] The Kennedy research group has made key advances in islet secretion sampling using microfluidics with a competitive, fluorescent immunoassay; islet secretions were sampled and repeatedly injected into an on-chip electrophoresis domain.[11-13] This approach has progressed from single-islet sampling[12] to parallel monitoring of 15 islets[11] at 10-second temporal resolution. A disadvantage of this method is its inherent complexity; secretion sampling requires pressure-based flow control with external pumps, microchip electrophoresis requires electroosmotic flow control with computer-controlled high-voltage power supplies, and fluorescence sensing requires a fluorescence microscope (or discrete optics). In addition, dramatic improvements in temporal resolution seem unlikely due to the nature of the required separation of antibodies with and without bound target. A recent advancement, using a clever device termed the "chemistrode," was reported by the Ismagilov group, in which droplet-based microfluidics was used to stimulate and sample chemical signals with pulses as short as 50 ms.[14] This system was applied to insulin secretion sampling from a pancreatic islet, at a temporal resolution of 1.5 s. Details on insulin secretion dynamics were not investigated in this work, likely due to the limited dynamic range of the assay.

In this work, we report a novel passive microfluidic droplet sampling method for quantifying pancreatic islet secretions, which allows approximately an order of magnitude improvement in temporal resolution (calculated based on diffusion/dispersion) compared to most commonly utilized methods[11,15], with similar resolution compared to the chemistrode.[14] In fact, this level of temporal resolution permits the observation that zinc ions are secreted from intact pancreatic islets in both short (~20-60 s) and long (~5-10 min) pulses, with the former mirroring the intraislet calcium oscillations that occur among β-cells of intact islets, and the latter mirroring insulin secretion measurements in the bloodstream.[15] This result is consistent with previous, qualitative results[16], while the quantitative nature of our approach provided further evidence for the Zn^{2+}/insulin co-secretion model.[15,17] Furthermore, this multiphase segmented flow approach (oil and aqueous phases; reviewed by Chiu and Lorenz[18]), combined with passively defined fluidic resistances, allowed accurate secretion sampling and quantitative measurements from single islets using a simple, handheld device and a fluorescence microscope. Device functionality was "programmed" into the fluidic channel pattern[19], such that secretion sampling and temporal segmentation were accomplished passively, and instrumentation requirements were minimized to the fluorescence microscope. At the same time, we have achieved unprecedented temporal resolution in quantitative sampling of secretions from small numbers of living cells. Thus, the approach should be more generally applicable to a variety of cellular systems.

Experimental

Reagents

Polydimethylsiloxane (PDMS) precursors, Sylgard® 184 elastomer base and curing agent, were obtained from Dow Corning. NaCl, KCl, $CaCl_2$, $MgCl_2$, HEPES, Triton-X, bovine serum albumin (BSA), fluorescein, silicone oil AR-20, EDTA, diazoxide (DZ), and D-glucose were purchased from Sigma-Aldrich (St. Louis, Missouri, United States). Fluo-4 acetoxymethyl (AM) ester, FluoZin-3 tetrapotassium salt, 1-1'-dioctadecyl-3,3,3',3'-tetramethylindocarbocyanine perchlorate (DiI), Gibco RPMI medium, phosphate buffered saline (PBS), and fetal bovine serum were also obtained from Invitrogen.

Microfluidic device fabrication

All devices were fabricated using polydimethylsiloxane (PDMS) as the channeled substrate and No. 1 glass coverslips as the floor substrate. Initial device design iterations were fabricated using a toner transfer masking (TTM) technique developed in-house.[20] The final device design was fabricated using standard soft lithography[21] with two different thicknesses of SU-8 photoresist (Microchem), as previously described for islet trapping.[2] The importance of this trapping technique for achieving high temporal resolution is emphasized in the text below. PDMS precursors were mixed thoroughly in a 10:1 ratio of elastomer:curing agent, poured over the master, degassed in a vacuum chamber, then cured for 2-3 hours at 70 °C. Cured PDMS was peeled from the master, and access holes were punched. The channeled surface and a glass cover slip were treated with an air plasma (Harrick Plasma; Ithaca, NY) for 60 s, then permanently bonded. Completed devices were then heated at 110 °C overnight to return channel surfaces to a hydrophobic state for aqueous-in-oil droplet formation. The channel pattern is shown in Fig. 1A, with dimensions and fluidic resistances reported in Table 1. Deeper islet-loading and calibration channels (R_{islet}, R_{cal}) were 125 μm deep, 300 μm wide, and 1.70 mm long. The shallow, droplet-forming region was fabricated at 35 μm depth, with the aqueous channels (R_{aq}) 50 μm wide and 39.50 mm long, and the oil channel (R_{oil}) 90 μm wide and 4.65 mm long. The common outlet (R_{out}) was 90 μm in width and 22.00 mm in length. Channel dimensions at the droplet-forming region were designed to produce droplets of approximately 180 μm length and 90 μm width, based, in part, on theory developed by the Whitesides group[22] (see text).

Pancreatic Islet Extraction, Sampling, and Staining

Islets were isolated as described previously[23-24] from live C57BL/6 mice (male) and maintained in RPMI medium containing 10 % fetal bovine serum, 11 mM glucose at 37 °C under humidified 5 % CO_2 for 24-48 h before imaging. Unless otherwise noted, “imaging medium” consisted of 125 mM NaCl, 5.7 mM KCl, 2.5 $CaCl_2$, 1.2 mM $MgCl_2$, 10 mM HEPES, 2 mM glucose, and 0.1% BSA at a pH of 7.4.

For secretion sampling and Zn^{2+} measurements, single isolated islets were first transferred from the RPMI culture medium into imaging medium (at 37 °C). After starving islets via 2 h equilibration in imaging medium with a basal glucose concentration of 2 mM, islets were loaded onto the microchip, which was held on a microscope stage in a humidified, temperature controlled chamber, maintained at 37 °C. During imaging, each islet was perfused continually with FluoZin-3- (0.2 μM) and EDTA- (10 μM) supplemented imaging medium at a vacuum driven flow rate of approximately 0.1 μL min^{-1}, as defined by the device fluidic resistances (see Microdevice Design section). A constant, stable vacuum pressure of 17 kPa was applied using an air-filled 20-mL syringe, with initial and final volumes defined by spacers (ideal gas law). Stability of applied vacuum was evident by the highly monodisperse droplet sizes, as well as the consistent aqueous flow rates achieved. Similar devices have been shown to provide more than adequate nutrients to the islets.[2] Zinc levels in islet secretions were imaged in this manner for up to 2 h. Stimulatory glucose levels (11 mM), with or without diazoxide (0.2 mM), were introduced by simply emptying the microfluidic well, adding glucose-supplemented imaging medium (with FluoZin-3 and EDTA), then pulling vacuum briefly at the R_{cal} inlet to allow rapid introduction of the stimulation.

In preparation for imaging of intercellular calcium ($[Ca^{2+}]_i$), isolated islets were stained with 4 μM Fluo-4 AM in imaging medium at room temperature for 2-3 h prior to imaging of $[Ca^{2+}]_i$ time course data. A single islet was loaded onto the microchip, which was held on a microscope stage in a humidified temperature controlled chamber, maintained at 37 °C. During imaging, each islet was perfused continually with imaging medium at a vacuum driven flow rate of ~0.1 μL min^{-1}. Stimulatory glucose levels (11 mM) were introduced as described above.

Image Acquisition and Analysis

Confocal fluorescence images of aqueous-in-oil droplets and pancreatic islets were acquired using an LSM 5Live line-scanning confocal microscope (Carl Zeiss) with either a 10× 0.5 NA Fluar or a 20× 0.8 NA Fluar objective. Fluorescein (visualization), FluoZin-3 (zinc measurement), or Fluo-4 (calcium measurement) fluorescence was imaged using a 488 nm diode laser for excitation and a 495-525 nm bandpass filter to detect fluorescence emission. Oil-soluble red fluorescent dye, DiI, was imaged using the same 488 nm diode laser for excitation (non-optimal), but with a 560-675 bandpass filter to detect fluorescence emission. Simultaneous imaging of green (495-525 nm) and red (560-675 nm) fluorescence was accomplished using two separate CCD arrays interfaced with the LSM 5Live through software (Carl Zeiss). All image analysis algorithms were written in-house using ImageJ[25] and Matlab. Further information is provided in the text (Fig. 2), and the Matlab code is included in Supplementary Information. It should be noted that a much simpler optical scheme (e.g. a laser, an objective, and two photomultiplier tubes with separate emission filter sets) would suffice for our method.

Calibration for Zn^{2+}

Off-chip calibrations were carried out in a spectrofluorometer, with excitation at 490 nm and emission measurement at 520 nm. Signal from Fig. 3A was collected by integrating emission and sampling at 1 Hz, and photobleaching was essentially negated using a 0.1 s lamp exposure time (10% duty cycle on excitation shutter). On the microfluidic device, prior to loading islets for secretion sampling experiments, calibrations were carried out daily at 37 °C (see Fig. 3C). Sequentially, Zn^{2+} calibration standards in FluoZin-3- and EDTA-free imaging medium (125 mM NaCl, 5.7 mM KCl, 2.5 $CaCl_2$, 1.2 mM $MgCl_2$, 10 mM HEPES, 2 mM glucose, and 0.1% BSA at a pH of 7.4) were added to the reservoir of the calibration channel, R_{cal}, and droplet formation was begun. The islet-loading channel, R_{islet}, contained FluoZin-3- and EDTA-supplemented imaging medium. Diffusive mixing of Zn^{2+} ions was confirmed to be complete (see Fig. 3C inset and Supplementary Information, Fig. S1). Mean values of Zn^{2+} concentration were calculated using the described image analysis methods. All calibration curves were fit to a monomolecular limited growth model by non-linear least squares analysis using OriginPro 8.

Results and Discussion

Droplet formation

Our approach to sampling secretions from single pancreatic islets was to utilize microfluidic channels to sample at low flow rates, while exploiting downstream aqueous-in-oil droplet formation to minimize dilution of secreted molecules. First, the droplet formation region was optimized. Several iterations were required to arrive at the final design as shown in Fig. 1A. Initial designs were fabricated using a recently-reported method by our group, termed toner transfer masking (TTM)[20], while the final design was fabricated using standard soft lithography. A key aspect of all designs was the incorporation of passive flow control[19] using fluidic resistances. Based on the simple scaling law developed by the Garstecki et al.[22], under certain geometric constraints, the length-to-width ratio (L/w) of droplets formed at a T-junction (Fig. 1A, lower inset) can be considered entirely a function of the oil and aqueous volumetric flow rates (Q_{oil} and Q_{aq})

$$\frac{L}{w}=1+\alpha\frac{Q_{aq}}{Q_{oil}} \quad (1)$$

where α is a geometrically-defined constant that is set equal to unity in this case. Eq. 1 clearly shows that with $Q_{aq} = Q_{oil}$, the droplets' $L/w = 2$. Although Garstecki et al. utilized syringe pumps to control their flow rates, our approach was to equate Q_{aq} and Q_{oil} passively, using fluidic resistors. A simple electrical circuit model of our microfluidic device is shown in Fig. 1B. Each channel is represented by a resistor. Since it was desirable to avoid syringe pumps and use only a single vacuum line at the outlet to control the flow, the relative flow rates Q_{aq} and Q_{oil} at the droplet forming T-junction were controlled passively by equating the fluidic resistances from each path. Since the viscosity of the silicone oil is 20 times larger than that of aqueous solution, the resistance of the aqueous path (combination of $R_{islet}/\underline{R_{cal}}$ and R_{aq}) was designed to be 20 times larger than R_{oil}. The various channel resistances, as labeled in Fig. 1B, are listed in Table 1. By assuming that our pressure source (analogous to a voltage source) in series with a fluidic resistor could approximate a source of constant volumetric flow rate (analogous to electrical current), we could invoke the fluidic analogy to Ohm's Law[19] and substitute the fluidic resistance values into Eq. 1, arriving at

$$\frac{L}{w}=1+\frac{2\,R_{oil}}{R_{islet}+2\,R_{aq}} \tag{2}$$

where the fluidic resistance values R_{oil}, R_{islet} (=R_{cal}), and R_{aq} are defined by Fig. 1A-B and Table 1. Substituting these values into Eq. 2, we obtain $L/w = 1.99$ (using resistances from either 25 °C or 37 °C). Aqueous segments of this size allowed high temporal resolution in secretion sampling from islets (*vide infra*).

As shown in Fig. 1C, the combination of the Garstecki scaling law (Eq. 1)[22] with passive fluidic flow control[19] resulted in formation of highly monodisperse droplets, with a relative standard deviation of only 1.98%. This experiment was conducted at 37 °C in a humidity-controlled incubator (secretion sampling conditions), and a constant vacuum of 17 kPa was applied to the outlet using a single, handheld 20-mL syringe. Thus, no syringe pumps or electrical components were required to achieve this level of precision. Image analysis of 3257 droplets revealed an average volume of 0.470 ± 0.009 nL (470 ± 9 pL). Remarkably, the average value of L/w over these experiments was 2.02 ± 0.07, showing near perfect correlation with Eq. 1, which predicted a $L/w = 1.99$. As shown in the analysis below, these droplets were ideal for collecting and measuring single islet secretions with high temporal resolution.

Secretion sampling with high temporal resolution

In order to sample secretions from single islets, then measure Zn^{2+} concentrations in droplets downstream using fluorescence, it was important that our devices could sample at a low enough volumetric flow rate to allow sufficient accumulation of the ions for detection with FluoZin-3 (K_d = 15 nM). Thus, overall fluidic resistance of the device was important in this case. On the other hand, to supply adequate nutrients to the islet and achieve high temporal resolution, the volumetric flow rate could not be reduced *ad infinitum*. As discussed herein, passive sampling (syringe-applied vacuum of 17 kPa) at a chosen aqueous volumetric flow rate of 0.100 mm^3 min^{-1} (0.100 μL min^{-1}) allowed a balance between Zn^{2+} detection sensitivity, islet survival, and temporal resolution within droplets.

First, Zn^{2+} detection sensitivity was considered in choosing the 0.100 μL min^{-1} aqueous volumetric flow rate. At this flow rate, typical insulin secretions from single islets under either basal or stimulatory glucose levels (10-100 pg $islet^{-1}$ min^{-1})[11,15] would result in downstream insulin concentrations in the range of 17-170 nM. Since two Zn^{2+} ions are co-crystallized into insulin hexamers within β-cell secretory granules[26], this 2:6 (Zn^{2+}:insulin) ratio was applied to calculate expected Zn^{2+} concentrations in the range of approximately 6-60 nM. Utilizing

FluoZin-3 (K_d = 15 nM) for fluorescence detection, the ideal Zn^{2+} concentration range would be 1.5-150 nM, which encompasses the expected range of islet secretions.

To ensure islet survival at this flow rate, the cross-sectional area of the islet confinement channel was optimized. Islets were confined within a microfluidic channel of 125 μm depth, similar to the diameter of the average islet.[4] The photomask design is shown in Fig. 1A. The cross-sectional area of the confinement channel was 0.0375 mm^2, resulting in an average linear flow velocity of 2.67 mm min^{-1} at a volumetric flow rate of approximately 0.100 mm^3 min^{-1}. This linear flow velocity resulted in complete replacement of solution surrounding the average islet (0.1-0.2 mm diameter) roughly 13 to 27 times per minute, which was sufficient for constant replenishment of nutrients to the confined cells, similar to results shown previously by our group.[2] In fact, this environment could be considered as a better approximation of the in vivo flow of blood through islet vasculature in the pancreas[10] than that of typical culture dish. Notably, it was possible to image islets for several hours without a detectable difference in secretory response, implying adequate islet survival for the experiments shown herein.

Temporal resolution was defined by the cross-sectional area of the collection channels, as well as the aqueous droplet lengths. Since the islet trapping region was defined by a decrease in channel depth from 125 μm to 35 μm, secretions were immediately swept from the confinement channel (R_{islet}, area = 0.0375 mm^2) into a collection channel (R_{aq}) with a cross sectional area of 1.75×10^{-3} mm^2, resulting in a 21.4-fold increase in linear flow velocity to ~57.1 mm min^{-1}. Based on the 39.50-mm length of the collection channel (required for flow rate control and mixing of calibration standards), the typical transit time for secretions from the islet to the droplet-formation region was, therefore, 42 s. In this case, diffusion and laminar dispersion[27] of zinc ions in only one dimension (parallel to the channel) would account for smoothing of the time traces prior to droplet formation. Using the average of reported diffusion coefficients of zinc ions in aqueous solutions at room temperature, 6.47×10^{-6} cm^2 s^{-1} 28, then adjusting to the value at 37 °C based on the viscosity ratio of water at 25 and 37 °C (0.890/0.686 = 1.30), a zinc ion diffusion coefficient, D, of 8.39×10^{-6} cm^2 s^{-1} at 37 °C was calculated. Accordingly, the effective diffusion coefficient, D , was calculated to be 4.18 × D_{eff} = 4.35×10^{-5} cm^2 s^{-1}, by considering laminar dispersion as a function of channel aspect ratio.[27] These calculations consider that three-dimensional laminar dispersion (vertical and horizontal gradients) due to pressure-driven flow through a rectangular channel dominates the smoothing of zinc pulses within the sampling channel (R_{aq}) over this time scale; diffusion and convection alone are insufficient to describe the smoothing.[27] With this value, it was then estimated that the 42 s transit time within the collection channel would result in a diffusion/dispersion length of 604 μm. At an average droplet length of 179 ± 4 μm, this value was equivalent to the length of 3.38 droplets. Such a diffusion/dispersion length should result in a three-dimensionally uniform Zn^{2+} concentration within each droplet at the point of fluorescence detection (observed throughout all experiments), allowing each droplet to serve as a discrete measurement of Zn^{2+} concentration over the temporal secretion profile. Considering again that the diffusion length was equivalent to 3.38 droplets, the discrete nature of the droplet measurements also implied that no less than four droplets should be averaged to represent a single time point. Separate measurement of <4 droplets would be an over-sampling of our signal (signal = bursts of Zn^{2+} secretions). At the average droplet production rate of 3.66 droplets s^{-1}, with each point represented by a minimum two droplets, our device was capable of measuring temporal Zn^{2+} secretion patterns at a minimum calculated resolution of 1.09 s.

Taken together, the results in this section suggest that the devices shown in Fig. 1A should be capable of sampling and measuring islet-secreted Zn^{2+} with high temporal resolution, comparable to the chemistrode-based measurements[14], while maintaining islet viability.

Image analysis

Using the high-speed, line-scanning confocal microscope (LSM 5Live, Carl Zeiss), droplets were imaged as they passed through the outlet microfluidic channel (R_{out}, Fig. 1A). Using a 20× 0.8 NA Fluar objective, with 4 × 4 binning of pixels, two 128 by 32 pixel images (red and green lines) were collected at 40 frames per second (fps). Due to the large amount of information required to sample islet secretions over approximately 1 h, secretion sampling data was collected in 10 min increments (note small gaps in traces in Fig. 4 and Fig. 6), resulting in file sizes of approximately 490 MB per 10 min. Processing of these large file sizes demanded a combination of ImageJ[25] and Matlab algorithms. ImageJ was used to crop images then convert from 12-bit RGB to 8-bit grayscale, and a Matlab algorithm was used to process this data (m-file text included in Supplementary information). It should be noted that a much simpler optical scheme (e.g. a laser, an objective, and two photomultiplier tubes with separate emission filter sets) would suffice for our method. In order to develop the present method, we chose to utilize the high-speed confocal imaging system to obtain information on the spatial distribution of droplet formation and propagation.

An example of the image analysis is shown in Fig. 2. Six-image montages (25 ms between images, top to bottom) from both the green (495-525 nm) and red (560-675 nm) fluorescence emission channels are shown in Fig. 2A and 2B, respectively, representing the typical 24 000 images that were recorded for each 10-min collection. Raw signal from the green channel (Fig. 2A) corresponds to the aqueous phase, with the highest intensities showing Zn^{2+}-bound FluoZin-3 during an islet secretion measurement. Raw signal from the red channel (Fig. 2B) corresponds to DiI-saturated silicone oil phase, a constant reference which provided a simple means for discriminating droplet signals from background signals, even with undetectable signal levels from the green channel. In this way, independent of the Zn^{2+} secretion signal, a continuous (40 fps) reference to background was possible. Using Matlab, the red channel ("oil signal") was normalized to the median of its signal over the 24 000 frames (Fig. 2C). This normalized oil signal was used to calculate 24 000 corresponding "mask" images for each 10-min collection. Sobel edge detection (derivative) kernels were used to detect droplet edges (Fig. 2D), which were used with the normalized oil signal to calculate binary aqueous (Fig. 2E) and oil (Fig. 2F) masks. These masks were used to discriminate between fluorescence signal and background in the green channel ("aqueous signal"). Akin to lock-in or phase-sensitive detection, the integrated aqueous signal from two or more droplets could then be digitally amplified over the background noise. Integrated background signals were subtracted from the amplified, integrated aqueous signals, at which time the calibration curve could be used to determine $[Zn^{2+}]$ (see below). This method was important in reducing microscope focal drift and laser power fluctuations, and all microfluidic sampling and Zn^{2+} secretion data presented herein were treated in this manner.

Zinc calibration and data handling

As described previously[16], quantitative detection of Zn^{2+} in real time using FluoZin-3 was challenging due to the relatively large concentrations of Ca^{2+} (2.5 mM) and Mg^{2+} (1.2 mM) ions in the imaging medium, ions which bind FluoZin-3 with low affinity. Furthermore, inconsistent background signals were detected in untreated water samples, likely due to trace levels of metals such as Fe^{2+} that bind FluoZin-3 with high affinity.[29] To circumvent this problem, we added 10 μM of the metal chelator EDTA to the imaging medium. First, the EDTA effectively reduced background signals from trace metals. Second, we exploited the relatively slow ligand exchange rate, where EDTA pre-saturated with Ca^{2+} and Mg^{2+} ions would take several minutes to chelate newly introduced Zn^{2+} ions. In other words, Zn^{2+} bursts in solution could be briefly detected by FluoZin-3 until they were chelated by EDTA. This concept was proven empirically at 19 °C using a spectrofluorometer (excitation 490 nm, emission 520 nm), as shown in Fig. 3A. Into 1.0 mL imaging medium, Zn^{2+} bursts were simulated by addition of

microliter-scale volumes of stock Zn^{2+}, followed by mixing for 5 seconds, then emission measurement over time. The data in Fig. 3A was fit to single exponential decay curves using nonlinear least squares fitting (OriginPro 8), and the decay lifetimes were 63.94 ± 0.91 s (n = 4). The pre-exponential factors from these fits were used to assemble the calibration curve in Fig. 3B ($r^2 = 0.9963$). These results provided evidence that for up to two minutes (**see** Fig. 3A), it was reasonable to assume that Zn^{2+} bursts in the expected concentration range could be detected before EDTA chelation of the Zn^{2+} ions reduced the signals to undetectable levels. In fact, after the 42-second delay between Zn^{2+} secretion and detection using our devices (Fig. 1A), the signal levels should be approximately 52% of maximal levels, which should be easily detectable. To confirm a similar response within the microfluidic system, a five-point calibration curve was carried out on the device, with final (mixed) values of 1, 3, 10, 32, and 100 nM Zn^{2+} (filled black squares, dashed black line, $r^2 = 0.9999$). Daily calibrations were limited to 3-point curves, with 3, 10, and 100 nM Zn^{2+} (open gray circles, solid gray line). As shown in Fig. 3C, the on-chip calibration curves were well-correlated within the range of Zn^{2+} concentrations of interest in this work. Diffusive mixing of Zn^{2+} ions was confirmed to be complete (see inset images and Supplementary Information, Fig. S1).

These calibration curves were used to determine the concentration for the final data processing step. Aqueous flow rates were measured by image analysis of the time lapse videos taken during secretion sampling. Imaged droplet areas were converted into volumes by multiplying by channel depth and accounting for edge curvature, resulting in an average aqueous volumetric flow rate of 103.1 ± 6.6 nL min^{-1} during secretion sampling experiments (approximated as 0.100 mm^3 min^{-1} in above calculations). This value equates to 3.66 droplets s^{-1} (3.66 Hz), giving a droplet every 0.274 s on average. Image analysis of fluorescence data was converted to concentration using the calibration curve shown in Fig. 3C. Multiplying by the volumetric flow rate, Zn^{2+} concentration could then be converted to mass flow rate of Zn^{2+} for each islet, in units of fg $islet^{-1}$ min^{-1}.

Quantitative zinc secretion measurements from starved islets

Droplet sampling devices were used to sample secretions from live C57BL/6 mouse islets. As shown in Fig. 4, quantitative Zn^{2+} secretions were measured during glucose stimulation. Islets Z1 and Z2 (different mice) were starved in 2 mM glucose for 2 h prior to analyses. For islet Z1 (Fig. 4A), upon stimulation with 11 mM glucose (G), Zn^{2+} secretion rose from ~40 fg $islet^{-1}$ min^{-1} to ~90 fg $islet^{-1}$ min^{-1}. After treatment with 0.2 mM diazoxide (DZ), a potassium channel activator that is know to cease intra-islet Ca^{2+} activity as well as insulin secretion, the islet Zn^{2+} secretion returned to basal levels. The high temporal resolution, combined with the quantitative nature of our method, allowed the simultaneous observation of slow (9.9 ± 2.0 min spacing, 8.7 ± 2.3 min plateau width) and rapid (38.7-s median period) Zn^{2+} oscillations. The slow pulses were consistent with typical observations of insulin secretion dynamics[11,15], while the period of the rapid pulses resembled that of intra-islet Ca^{2+} oscillations.[15] Inset plot shows the region between 52 and 60 s in the time trace, where several rapid Zn^{2+} pulses are evident; this data is analyzed further below (see Fig. 5B). Based on the 2:6 (Zn^{2+}:insulin) molar crystallization ratio, we calculated the corresponding insulin levels to be ~10 pg $islet^{-1}$ min^{-1} basal and ~30 pg $islet^{-1}$ min^{-1} after stimulation (right axis in Fig. 4A). These values fell within the expected range of single-islet secretions, based on previous reports.[11,15]

Sampling from islet Z2 (Fig. 4B) showed similar behavior. Zn^{2+} mass flow rate increased from ~40 fg $islet^{-1}$ min^{-1} to ~80 fg $islet^{-1}$ min^{-1}, then dropped as low as ~15 fg $islet^{-1}$ min^{-1} after diazoxide (DZ) treatment. Slow pulses were spaced by 9.3 ± 0.8 min, with 9.7 ± 2.1 min plateau widths. Rapid bursts were observed at a median period of 23.6 s. Calculated insulin levels are represented by the right axis in Fig. 4B. A third starved islet (islet Z5) that was treated with a

change from 2 mM to 11 mM glucose over a shorter time period (20 min) showed similar increases in secretory activity (Supplementary Information, Fig. S2A).

Intra-islet calcium oscillations

Glucose-stimulated insulin secretion in pancreatic β-cells is known to progress through glucose metabolism, membrane depolarization, Ca^{2+} influx, then to exocytosis of insulin and Zn^{2+} containing granules. To confirm our hypothesis that the observed rapid Zn^{2+} burst periods measured with our system (Fig. 4) were related to intraislet Ca^{2+} oscillations, islets were starved in 2 mM glucose, stained with Fluo-4, then imaged. Fig. 5A shows the results of these measurements from two islets (C1 and C2, from different mice), where the fluorescence intensity was measured by simply integrating the signal from the entire islet. Upon stimulation from 2.0 to 11.0 mM glucose (G) at time zero, the islets first responded by asynchronous bursts, when the Ca^{2+} levels in the β-cells began to oscillate in a coordinated fashion throughout the islet, consistent with previous reports.[2-3,15] By measuring the spacing between oscillation maxima, the median oscillation period for each islet was determined to be 34.8 (islet C1) and 31.5 s (islet C2) (Fig. 5B, top), values that were within the typically-measured range of oscillation periods for different mice.[30] Firstly, these data indicated that extracted islets were viable. Secondly, a comparison of Ca^{2+} oscillation periods with Zn^{2+} burst periods (Fig. 5B, bottom) revealed a close resemblance. Although fewer numbers of bursts were available for analysis, median burst periods of Zn^{2+} were measured to be 38.7 (islet Z1) and 23.6 s (islet Z2), values that encompassed the range of intra-islet Ca^{2+} oscillations. This observations were consistent with previous reports[16], which showed a qualitative match between islet Ca^{2+} oscillations and Zn^{2+} secretion pulses, where the authors imaged an islet that was stained with Ca^{2+}-indicator and bathed in Zn^{2+}-indicator dye.

Zinc secretion from unstarved islets

Secretions from islets Z3 and Z4 (different mice) were taken under different conditions than that shown above. Neither islet was starved in 2 mM glucose, thus both were transferred from culture medium (11 mM glucose) into imaging medium (11 mM glucose) and incubated at 37 °C for 2 h prior to analyses. Secretions from islet Z3 during maintained glucose stimulation were sampled in the microfluidic device for 52 min, then the islet was exposed to 0.2 mM diazoxide (DZ) and sampled for another 20 min (Fig. 6A). In this case, the mass flow rates of Zn^{2+} secretion reached levels as high as ~800 fg islet^{-1} min^{-1}, significantly larger than the ~100 fg islet^{-1} min^{-1} bursts observed with starved islets. Islet Z3 showed very few detectable rapid oscillations, while the slow pulses (11.4 ± 6.9 min spacing, 12.0 ± 3.6 min plateau width) again matched with typical observations of insulin secretion dynamics. Secretions from islet Z4 showed a similar effect of larger mass flow rates, with bursts of nearly 500 fg islet^{-1} min^{-1} (Fig. 6B). Note that the treatment procedure was again modified. Islet Z4 was never treated with DZ, but after 41.5 min of 11 mM glucose treatment, the glucose levels were reduced to 2 mM. Observed oscillation periods were also slightly smaller (faster oscillations) with islet Z4. Slow oscillations were observed with 6.5 ± 2.8 min spacing and 6.1 ± 1.2 min plateau width, although these values were again within previously observed ranges. Interestingly, islet Z4 seemed to show an irregularly large number and magnitude of rapid Zn^{2+} bursts, with a median oscillation period of 19.5 s (histogram inset in Fig. 6B), and with changes as large as 369 fg islet^{-1} min^{-1} occurring in a span of only 13 s (slope of ~1700 fg islet^{-1} min^{-2}). Although this observation was only made on a single islet, it is noteworthy that irregular islet secretion patterns have also been observed by other groups.[11] A third unstarved islet (islet Z6) that was treated with 0.2 mM diazoxide at 11 mM glucose over a shorter time period (20 min) showed a similar decrease in secretory activity (Supplementary Information, Fig. S2B). Basal Zn^{2+} secretion rates (under diazoxide treatment or at 2 mM glucose) were higher for all three unstarved islets Z3, Z4, and Z6 (~100 fg islet^{-1} min^{-1}) than for the starved islets Z1, Z2, and Z5 (~40 fg islet^{-1} min^{-1}).

Conclusions

The novel approach to measuring islet zinc secretion described here leverages the benefits of microfluidic sampling and the sensitivity of fluorescence detection, yet minimizes the need for instrumentation complexity compared to previous methods.[11,15,17] Pre-experiment set up time for these passive devices is on the order of five minutes, making them essentially ready-to-use devices, permitting studies on biological systems such as the pancreatic islets investigated here. At the same time, the temporal resolution achieved has allowed unique, quantitative and qualitative observations of the islet secretory profile. Measured Zn^{2+} mass flow rates from islets corresponded well with expected insulin secretion levels (~10-100 pg $islet^{-1}$ min^{-1})[11, 15], when calculated using the 2:6 molar ratio (Zn^{2+}:insulin). These data, along with the similarities of Zn^{2+} pulse periods with intra-islet Ca^{2+} oscillations, provide cohesive evidence to strengthen the correlation between Zn^{2+} secretion and glucose-stimulated insulin secretion, mediated by intraislet Ca^{2+} oscillations. Thus, our technique should be useful for further studies on zinc homeostasis or paracrine signaling in pancreatic islets.

One disadvantage of the present method is that islets must be analyzed in serial fashion. For future analyses, it is clear that the device should be scaled up to allow parallel sampling from multiple islets, akin to the work by Dishinger et al.[11] Otherwise, statistically relevant observations to study, for example, zinc transporter knockout mice[31-32] would require a large time investment. Of course, the passive nature of our device should be highly amenable to scaling, since there are virtually no requirements for scaling the instrumentation, other than additional tubing. Future studies could also be focused on simultaneous measurement of zinc secretion and calcium oscillations.[15-17] In order to accomplish this, the geometry of the system must be reconfigured to allow imaging of the droplets in the same field of view as the islet. Finally, as direct detection methods or fluorescent sensors for other islet secretions (insulin, glucagon, somatostatin, etc.) are developed[33], our user-friendly device for passive droplet-sampling will permit unprecedented temporal resolution of the function of islets as individuals.

Supplementary Material

Refer to Web version on PubMed Central for supplementary material.

Acknowledgments

Support for this work was provided by award numbers F32DK07964 (Easley), R01DK053434 (Piston), and P20GM072048 (Piston) from the National Institutes of Health. Support was also provided by the Department of Defense Medical Free-Electron Laser Program. The authors would like to thank the Vanderbilt Institute for Integrative Biosystem Research and Education (VIIBRE) for use of their cleanroom facilities for device fabrication.

References

1. Göpel S, Kanno T, Barg S, Galvanovskis J, Rorsman P. J. Physiol 1999;521:717–728. [PubMed: 10601501]
2. Rocheleau JV, Remedi MS, Granada B, Head WS, Koster JC, Nichols CG, Piston DW. PLoS Biol 2006;4:e26. [PubMed: 16402858]
3. Benninger RKP, Zhang M, Head WS, Satin LS, Piston DW. Biophys. J 2008;95:5048–5061. [PubMed: 18805925]
4. Jo J, Choi MY, Koh DS. Biophys. J 2007;93:2655–2666. [PubMed: 17586568]
5. Butler AE, Janson J, Soeller WC, Butler PC. Diabetes 2003;52:2304–2314. [PubMed: 12941770]
6. Goss JA, Schock AP, Brunicardi FC, Goodpastor SE, Garber AJ, Soltes G, Barth M, Froud T, Alejandro R, Ricordi C. Transplantation 2002;74:1761–1766. [PubMed: 12499894]
7. Gunawardana SC, Benninger RK, Piston DW. Am. J. Physiol. Endocrinol. Metab 2009;296:E323–332. [PubMed: 19066321]

8. Suckale J, Solimena M. Frontiers Bioscience 2008;13:7156–7171.
9. Cabrera O, Berman DM, Kenyon NS, Ricordi C, Berggrern PO, Caicedo A. Proc. Natl. Acad. Sci. USA 2006;103:2334–2339. [PubMed: 16461897]
10. Nyman LR, Wells KS, Head WS, McCaughey M, Ford E, Brissova M, Piston DW, Powers AC. J. Clin. Invest 2008;118:3790–3797. [PubMed: 18846254]
11. Dishinger JF, Reid KR, Kennedy RT. Anal. Chem 2009;81:3119–3127. [PubMed: 19364142]
12. Roper MG, Shackman JG, Dahlgren GM, Kennedy RT. Anal. Chem 2003;75:4711–4717. [PubMed: 14674445]
13. Shackman JG, Dahlgren GM, Peters JL, Kennedy RT. Lab Chip 2005;5:56–63. [PubMed: 15616741]
14. Chen D, Du W, Liu Y, Liu W, Kuznetsov A, Mendez FE, Philipson LH, Ismagilov RF. Proc. Natl. Acad. Sci. USA 2008;105:16843–16848. [PubMed: 18974218]
15. Gilon P, Ravier MA, Jonas JC, Henquin JC. Diabetes 2002;(Suppl 1):S144–S151. [PubMed: 11815474]
16. Qian WJ, Peters JL, Dahlgren GM, Gee KR, Kennedy RT. Biotechniques 2004;37:922–933. [PubMed: 15597541]
17. Bergsten P, Hellman B. Biochem. Biophys. Res. Commun 1993;192:1182–1188. [PubMed: 8507191]
18. Chiu DT, Lorenz RM. Acc. Chem. Res 2009;42:649–658. [PubMed: 19260732]
19. Leslie DC, Easley CJ, Seker E, Karlinsey JM, Utz M, Begley MR, Landers JP. Nature Phys 2009;5:231–235.
20. Easley CJ, Benninger RKP, Shaver JH, Head WS, Piston DW. Lab Chip 2009;9:1119–1127. [PubMed: 19350094]
21. McDonald JC, Duffy DC, Anderson JR, Chiu DT, Wu H, Schueller OJ, Whitesides GM. Electrophoresis 2000;21:27–40. [PubMed: 10634468]
22. Garstecki P, Fuerstman MJ, Stone HA, Whitesides GM. Lab Chip 2006;6:437–446. [PubMed: 16511628]
23. Scharp DW, Kemp CB, Knight MJ, Ballinge WF, Lacy PE. Transplantation 1973;16:686–689. [PubMed: 4201956]
24. Stefan Y, Meda P, Neufeld M, Orci L. J Clin Invest 1987;80:175–183. [PubMed: 3110211]
25. Abramoff MD, Magelhaes PJ, Ram SJ. Biophotonics International 2004;11:36–42.
26. Dunn MF. BioMetals 2005;18:295–303. [PubMed: 16158220]
27. Doshi MR, Daiya PM, Gill WN. Chem. Eng. Science 1978;33:795–804.
28. Kariuki S, Dewald HD. Electroanalysis 2005;8:307–313.
29. Gee KR, Zhou ZL, Qian WJ, Kennedy R. J. Am. Chem. Soc 2002;124:776–778. [PubMed: 11817952]
30. Nunemaker CS, Zhang M, Wasserman DH, McGuinness OP, Powers AC, Bertram R, Sherman A, Satin LS. Diabetes 2005;54:3517–3522. [PubMed: 16306370]
31. Pound LD, Sarkar SA, Benninger RKP, Wang Y, Suwanichkul A, Shadoan MK, Printz RL, Oeser JK, Lee CE, Piston DW, McGuinness OP, Hutton JC, Powell DR, O'Brien RM. Biochem. J 2009;421:371–376. [PubMed: 19450229]
32. Nicolson TJ, Bellomo EA, Wijesekara N, Loder MK, Baldwin JM, Gyulkhandanyan AV, Koshkin V, Tarasov AI, Carzaniga R, Kronenberger K, Taneja TK, da Silva XG, Libert S, Froguel P, Scharfmann R, Stetsyuk V, Ravassard P, Parker H, Gribble FM, Reimann F, Sladek R, Hughes SJ, Johnson PR, Masseboeuf M, Burcelin R, Baldwin SA, Liu M, Lara-Lemus R, Arvan P, Schuit FC, Wheeler MB, Chimienti F, Rutter GA. Diabetes. Jun 19;2009 (Epub ahead of print)
33. Guillo C, Roper MG. Electrophoresis 2008;29:410–416. [PubMed: 18080249]

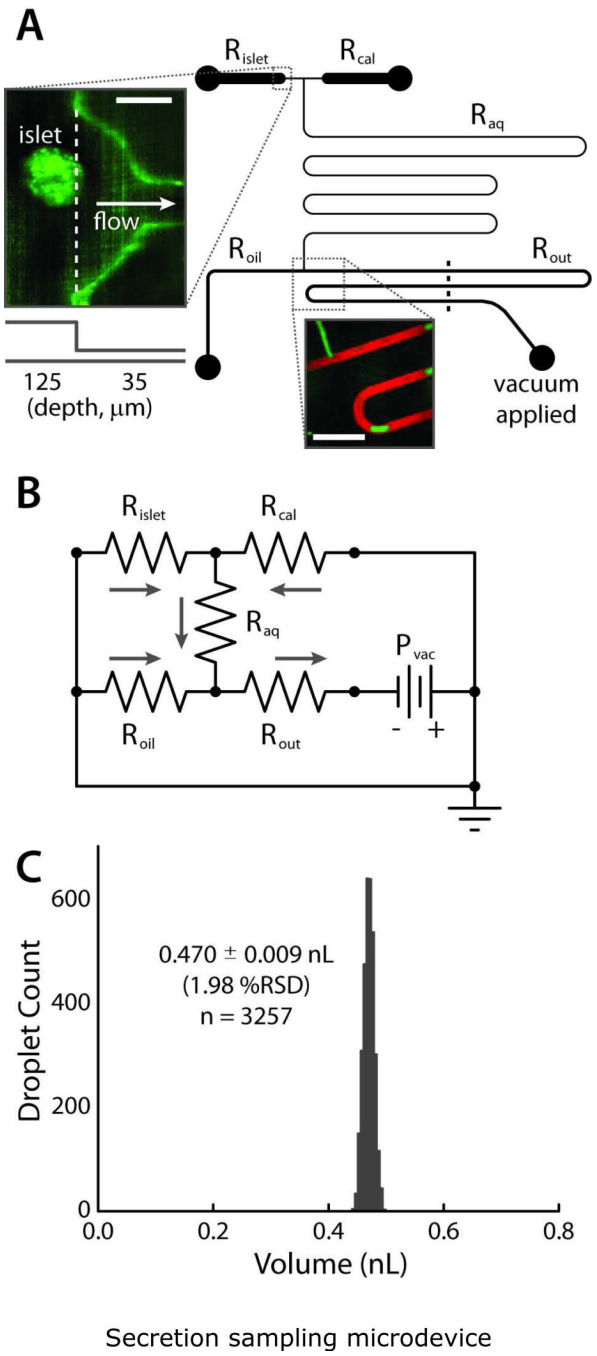

Figure 1.

Secretion sampling microdevice. (**A**) Channel layout with viewpoint from the top of device, with five categories of channels: islet loading/trapping (R_{islet}), calibration (R_{cal}), aqueous (R_{aq}), oil (R_{oil}), and outlet (R_{out}). Upper inset shows a confocal fluorescence image of an islet in the trapping region (scale bar 100 μm). Lower inset shows an image during droplet formation (scale bar 500 μm). Aqueous phase contains fluorescein (green), and oil phase DiI (red). Device is operated by simply applying vacuum to outlet with a handheld syringe. (**B**) Fluidic resistances (Table 1) were modeled using the electrical circuit analogy, allowing accurate, passive control of relative aqueous and oil flow rates (Q_{aq}, Q_{oil}). (**C**) The device was capable

of passively forming monodisperse populations of sub-nanoliter, aqueous-in-oil droplets at less than 2% relative standard deviation in volume (n = 3257).

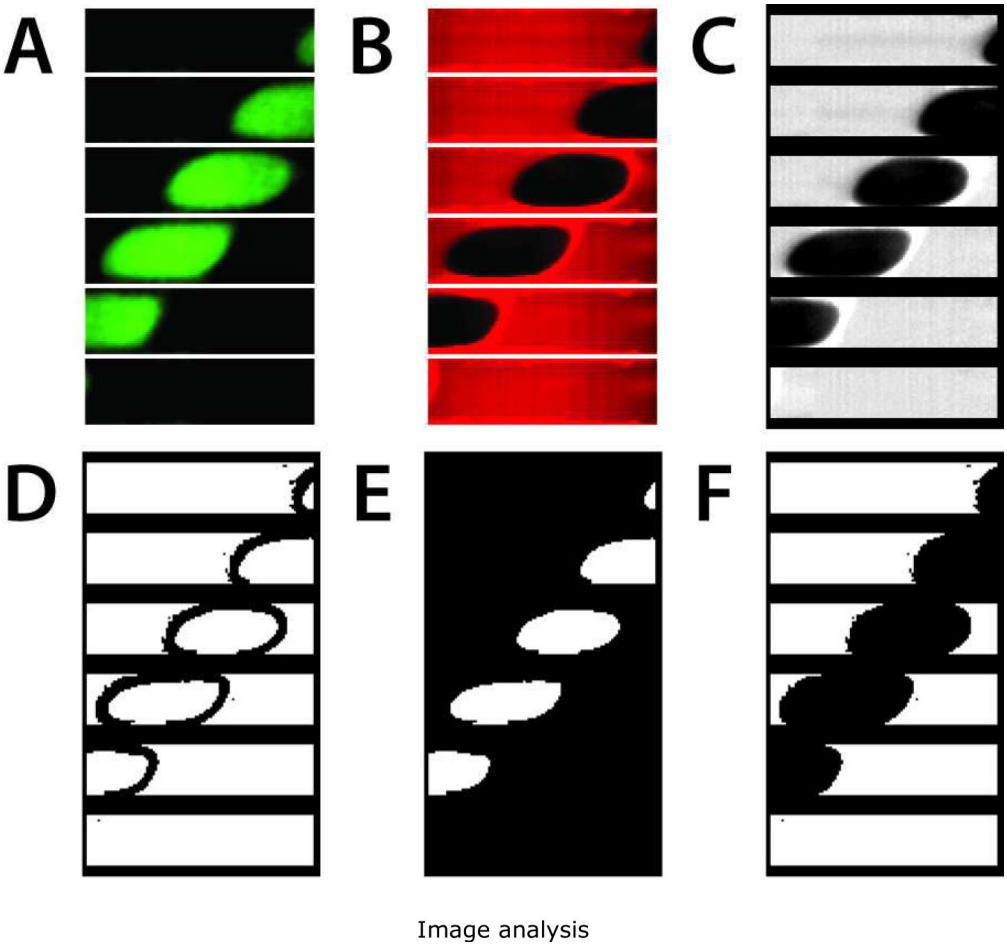

Figure 2.

Sequential examples of image analysis. Six frames of time-lapse data are shown (25 ms between frames, top to bottom), representing the typical 24 000 frames per 10 min acquisition. (**A**) Raw fluorescence emission from 495-525 nm, with signal arising from the aqueous phase Zn^{2+} bound to FluoZin-3 during islet secretion sampling. (**B**) Raw fluorescence emission from 560-675 nm, arising from the DiI-saturated oil phase, served served as a reference for droplet detection. (**C**) Normalized oil phase signal. (**D**) Edge detection algorithms were used to determine binary (**E**) aqueous and (**F**) oil masks for discrimination of signal from background, providing a continuous reference signal akin to lock-in detection.

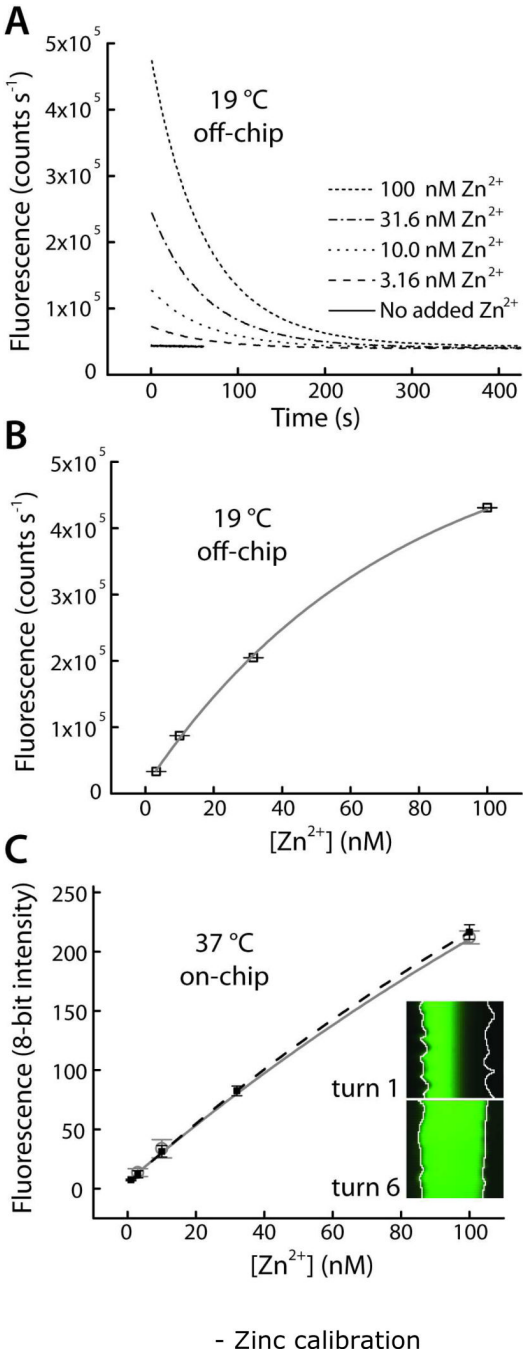

Figure 3.

Calibration for quantitative fluorescence detection of Zn^{2+} using FluoZin-3. (**A**) Ligand exchange rate of EDTA, pre-saturated with Ca^{2+} and Mg^{2+} ions in the imaging buffer, allowed brief observation of Zn^{2+} bursts. Collected at 19 °C with a spectrofluorometer (excitation 490 nm, emission 520 nm). (**B**) Data from (**A**) was fit to single exponential decay curves (lifetimes of 63.94 ± 0.91 s). Pre-exponential factors provided a calibration curve versus initial Zn^{2+} concentration (r^2 = 0.9963). (**C**) On-chip calibration (filled black squares, dashed black line, r^2 = 0.9999) and a typical daily calibration curves (open gray circles, gray line) collected in the microfluidic droplet sampling device at 37 °C. Inset shows that laminar separation of

Zn^{2+} and Zn^{2+}-free buffer at turn 1 of the microdevice was removed by diffusive mixing by turn 6, prior to droplet formation and calibration.

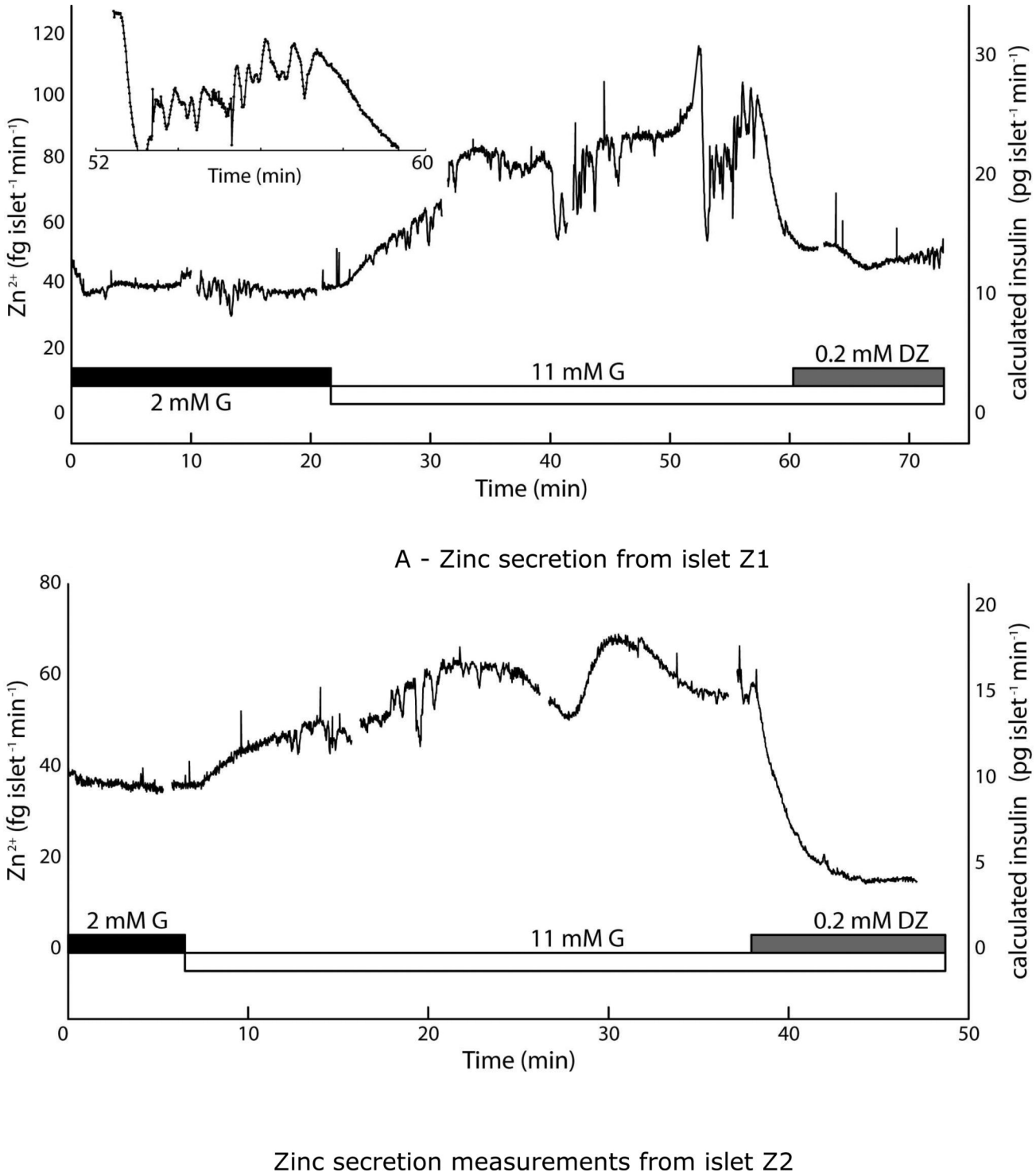

Figure 4.

Quantitative Zn^{2+} secretion measurements from live murine islets using the microfluidic droplet sampler. Islets were starved in 2 mM glucose for 2 h prior to analysis. (**A**) Upon stimulation from 2 to 11 mM glucose (G), Zn^{2+} secretion from islet Z1 rose from a basal level of ~40 fg $islet^{-1}$ min^{-1} to ~90 fg $islet^{-1}$ min^{-1}, then returned to basal levels upon treatment with the potassium channel activator diazoxide (DZ). Observed slow oscillations (9.9 ± 2.0

min spacing, 8.7 ± 2.3 min plateau width) resembled well-characterized slow insulin pulses. Inset data highlights rapid Zn^{2+} bursts, with median period of 38.7 s. (**B**) Similar behavior was seen with an islet from a second mouse (islet Z2) as well as from a third islet (Z5, Fig. S2A). Calculated insulin levels, based on the 2:6 (Zn^{2+}:insulin) crystallization ratio are shown on secondary y-axes (right).

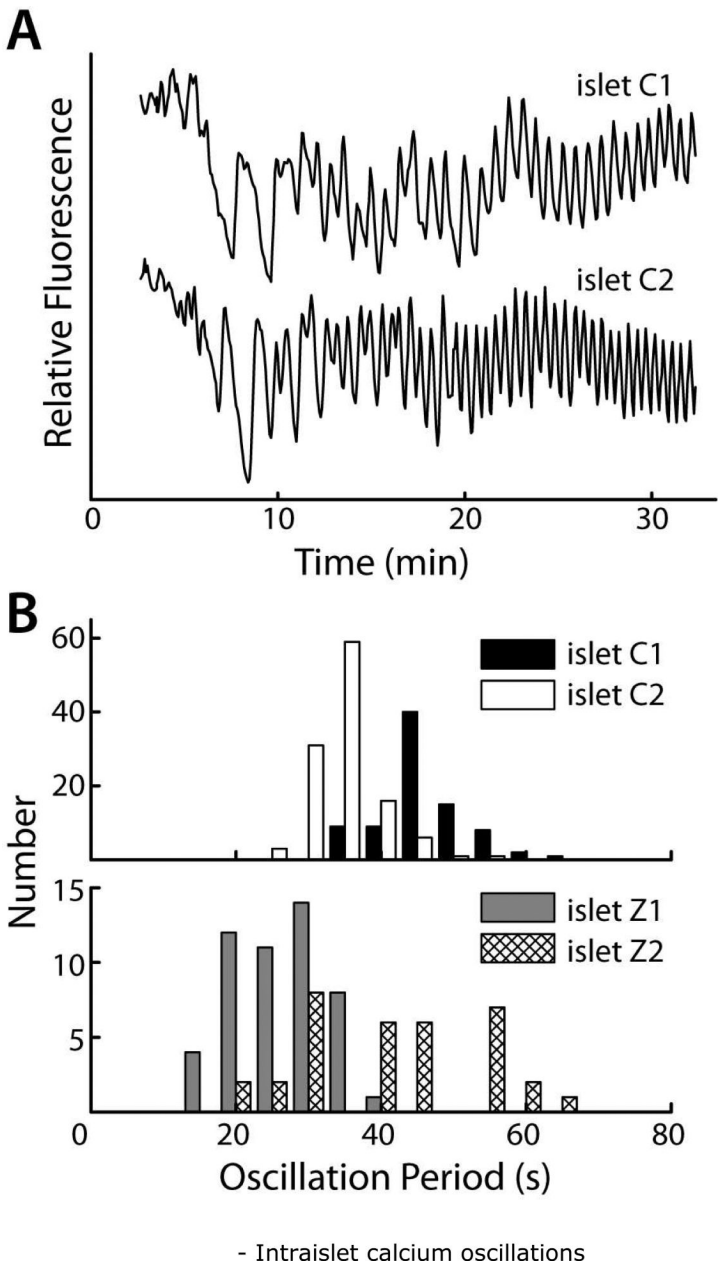

- Intraislet calcium oscillations

Figure 5.

Intraislet Ca^{2+} oscillations were imaged via confocal fluorescence microscopy after staining islets with Fluo-4 (Ca^{2+} indicator dye). Beta cells within the islet coordinated their oscillations following stimulation. (**A**) Integrated fluorescent intensities from whole islets, shown over time for islets C1 and C2 (different mice). (**B**) Distributions of intraislet Ca^{2+} oscillation periods from (**A**) match with periods of Zn^{2+} secretion bursts from islets Z1 and Z2.

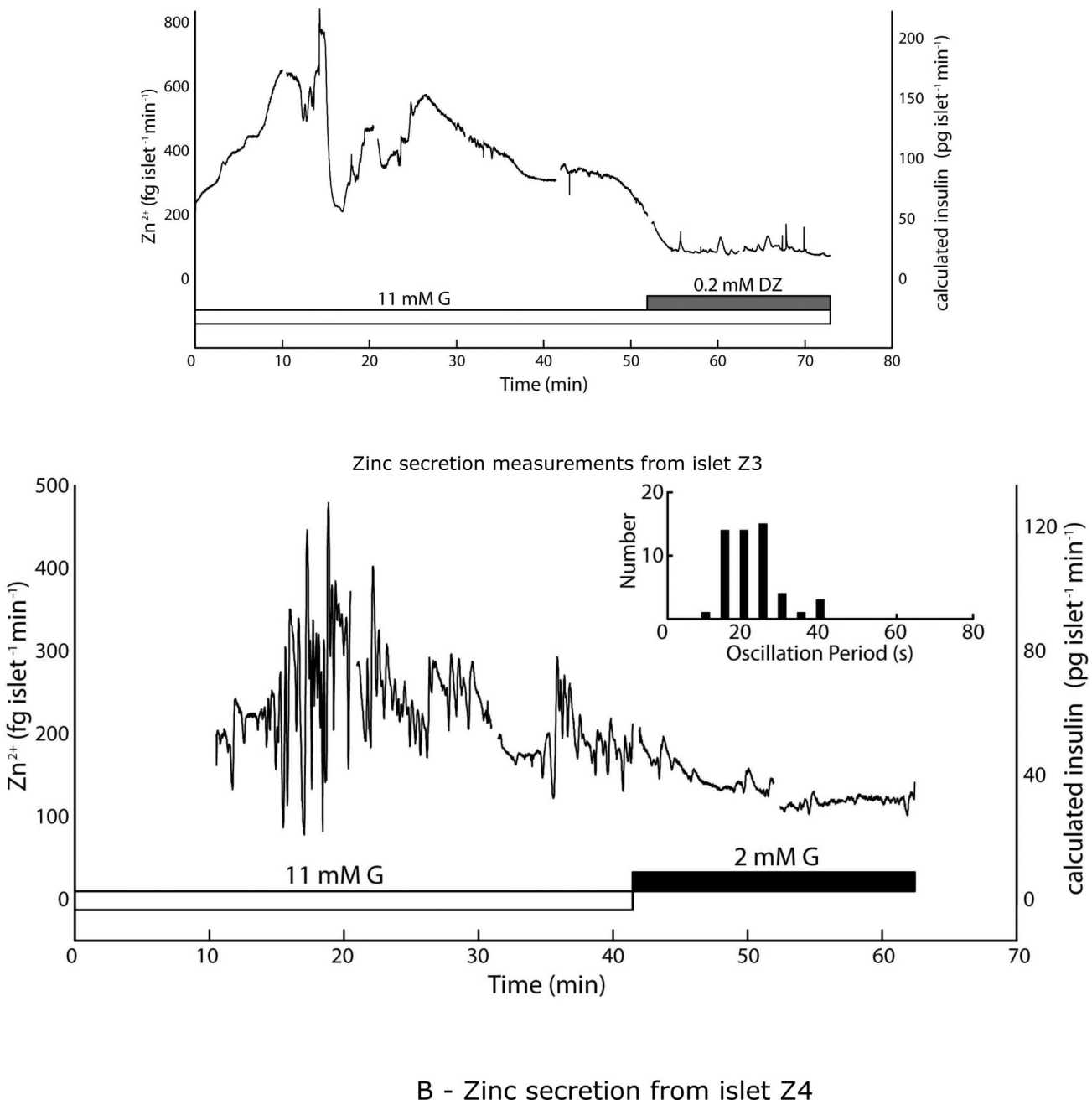

Figure 6.

Unstarved islets exhibited larger rates of Zn^{2+} secretion, as high as ~800 fg $islet^{-1}$ min^{-1}, while again showing Zn^{2+} secretion patterns that tracked with expected insulin secretion responses. Islets were pre-incubated in 11 mM glucose (G) for 2 h prior to sampling and imaging. (**A**) Secretions from islet Z3 were sampled in the droplet device for 52 min under stimulatory (11 mM) G, then under exposure to 0.2 mM diazoxide, which reduced Zn^{2+} secretion levels. A comparable response was observed from islet Z6 (Fig. S2B). (**B**) Islet Z4 was sampled for 31 min in 11 mM G, then switched to 2 mM G, which reduced Zn^{2+} secretion. Rapid, irregularly intense secretion patterns (histogram inset) were observed from this islet. Calculated insulin levels, based on the 2:6 (Zn^{2+}:insulin) crystallization ratio are shown on secondary y-axes (right).

Table 1

Channel dimensions for the device shown in Fig. 1A. Fluidic resistances (*R*) were defined by the channel cross-sectional area, length, shape, and fluid viscosity. The viscosity values used for water and silicone oil were 0.89×10^{-6} and 17.8×10^{-6} kPa s, respectively.

Resistor	Length (mm)	Width (mm)	Depth (mm)	Resistance (kPa s mm^{-3}) 25 ° C	37 °C
R_{islet} *	1.70 / 0.50	0.30 / 0.05	0.125 / 0.035	4.41	3.40
R_{aq}	39.50	0.05	0.035	345	266
R_{oil}	4.65	0.09	0.035	344	265
R_{out}	22.00	0.09	0.035	1630	1260

* Values for R_{cal} are equivalent to values shown for R_{islet}.